5-2024

Electrocatalytic Degradation of Bisphenol a Using Nickel Sulfide Supported on Graphene Oxide and Cobalt Sulfide Supported on Graphene Oxide Composite Materials

Katherine Ellynn Wright
The University of Texas Rio Grande Valley

ELECTROCATALYTIC DEGRADATION OF BISPHENOL A USING NICKEL SULFIDE SUPPORTED ON GRAPHENE OXIDE AND COBALT SULFIDE SUPPORTED ON GRAPHENE OXIDE COMPOSITE MATERIALS

A Thesis

by

KATHERINE ELLYNN WRIGHT

Submitted in Partial Fulfillment of the

Requirements for the Degree of

MASTER OF SCIENCE

Major Subject: Chemistry

The University of Texas Rio Grande Valley

May 2024

ELECTROCATALYTIC DEGRADATION OF BISPHENOL A USING NICKEL SULFIDE SUPPORTED ON GRAPHENE OXIDE AND COBALT SULFIDE SUPPORTED ON GRAPHENE OXIDE COMPOSITE MATERIALS

A Thesis
by
KATHERINE ELLYNN WRIGHT

COMMITTEE MEMBERS

Dr. Jason G. Parsons
Chair of Committee

Dr. Arnulfo Mar
Committee Member

Dr. Evangelia Kotsikorou
Committee Member

May 2024

ABSTRACT

Wright, Katherine E., Electrocatalytic Degradation of Bisphenol A Using Nickel Sulfide Supported on Graphene Oxide and Cobalt Sulfide Supported on Graphene Oxide Composite Materials. Master of Science (MS), May 2024, 43 pp., 1 tables, 22 figures, 37 references.

The degradation of bisphenol A (BPA) by nickel sulfide supported on graphene oxide (NiS/GO) and cobalt sulfide supported on graphene oxide (CoS/GO) composite materials was investigated. The catalysts were studied to determine the optimal conditions for BPA degradation using electrocatalysis. Electrolytic trials were performed using varying parameters, which included electrolyte concentrations of 1.0 g/L, 2.0 g/L, and 4.0 g/L Na_2SO_4, pHs of 2, 4, and 6, and constant currents of 0.100 A or 0.200 A. During the reaction, samples were taken before the current was applied and 30 minutes and 60 minute intervals to observe the degradation of BPA with respect to time. The synthesized catalyst samples were analyzed using both XRD and SEM. The SEM was used to analyze the electrode after the reaction. The degradation of the BPA was followed using HPLC, and the reaction products were identified using LC-MS/MS/MS. All the degradation reactions showed first-order kinetics for the degradation of BPA.

DEDICATION

The completion of my master's studies would not have been possible without the love, support, and guidance provided by my parents, Douglas and Sara Wright. I would also like to thank Timothy Wright, Bethany Wright, and Adam Rodriguez, for your actions, inspiration, and motivation. Thank you all for your love and patience, for this accomplishment would not have been possible without you.

ACKNOWLEDGEMENTS

I would like to express my absolute gratitude to Dr. Jason Parsons, chair of my committee, for your mentorship and guidance that has driven my maturation as a student. The countless hours invested into my research, encouragement, and infinite patience will not be forgotten. A big thanks to my thesis committee members: Dr. Evangelia Kotsikorou and Dr. Arnulfo Mar. Their advice and comments on my thesis helped to ensure the quality of my work.

I would also like to thank my fellow lab members, for their friendship and support has helped me through countless instances. Thank you all, for this accomplishment would not have been possible without you.

TABLE OF CONTENTS

LIST OF FIGURES

Page

CHAPTER I

BACKGROUND

Characteristics of Bisphenol A

Bisphenol A (2,2-Bis(4-hydroxyphenyl) propane, BPA); CAS # 80-05-7; is associated with epoxy resins and polycarbonates in commercial plastic synthesis. BPA belongs to a class of diphenylmethanes where two methyl groups replace the methylene hydrogens. BPA is a crucial intermediate organic monomer in the synthetic manufacturing of polymers and plastics, powder and liquid paints, dental fillings and sealants, packaging of food and beverages, as well as many other products, and has been found in trace amounts within the products[1, 2, 3, 4]. On average 3 million metric tons are generated annually, with an estimated annual growth rate of 3.5%, which has the potential to contaminate the environment[5].

Considerable amounts of BPA have migrated into the environment, through manufacturing of products (i.e. by-products), improper synthesis waste management, and from the general use of materials containing BPA. BPA is readily biodegradable in water, with a water solubility of 300mg/L at 25°C, and has a high stability, bioavailability, and motility in soils. These properties are due to its low volatility and atmospheric half-life of 7 days in water and 3 days in soils, causing moderate to insignificant levels in environmental samples. BPA falls into the class of chemicals called persistent organic pollutants (POPs) being released into the environment also presents uncertainty towards humans, wildlife, and marine life. BPA is a non-steroidal xenoestrogen, meaning it expresses hormonal properties by mimicking estrogen within

the body or inhibiting endogenous estrogen processes and this is also known as an endocrine disrupting chemical[8,9].

History and Use

The first synthesis of BPA occurred in 1905 in Germany by Thomas Zinke. Polycarbonate manufacturers in 1953 mentioned the earliest use of BPA as a starting material. The commercial production of BPA based polymers began in 1957 in the United States[6]. The first approved usage of BPA by the Food and Drug Administration for commercial polycarbonate production was in the early 1960s. In the early 2000s concern regarding the safety of BPA was heightened. The FDA confirmed the safety of the chemical found in material contacting food in August 2008. The FDA's science subcommittee questioned the recent report regarding assurance of the chemical by late October 2008. Also in late October 2008, a petition regulating prohibition of BPA in food packaging was submitted by the National Resource Defense Council, which was conclusively denied by the FDA in March 2012. Unconvinced, a four-year inspection of BPA toxicity began in fall 2014 by experts throughout the agency, ultimately giving the FDA no warrant to revise the food packaging safety assessment[7]. Monitoring POPs has been emphasized over the past 10 years due to emerging concern over the anticipated environmental risk among the ecosystem[8].

Still today, numerous products contain BPA including polycarbonate plastic and epoxy resin production including water bottles, food packaging, powder and liquid paints, dental fillings and sealants, adhesives, coatings, finishes, lenses, medical devices, automobile parts, etc.[9]

Environmental Fate and Toxicity of BPA

Toxicity of BPA has been extensively studied in waters, food, with in rats, humans, and other living organisms to understand the compounds absorption, excretion, and metabolization. Most BPA found in the environment is in sewage or liquid waste flowing into rivers and seas from the processing of materials containing the compound. Although the levels of contamination are typically minimal, there is a continuous supply of BPA entering the environment everyday due to nonstop production[9]. The Journal of Xenobiotics showed a study of a wastewater treatment plant that received 580 g/day BPA, 24% of which collected in surface waters. Using physicochemical treatment, however, only 76% of the BPA was removed from the aqueous phase. The BPA concentration not removed from the waste, has been shown to collect in the aquatic environment due to sewage and liquid discharge[11].

The majority of human exposure originates from dietary contact with products containing BPA residues. Contamination levels vary among different foods with significant concentrations detected in canned foods and lower BPA concentrations found in fresh or frozen foods. Primarily, BPA contamination originates from migration from the plastic internal coating of the can into the foodstuff[9,12]. Animal sourced foods have also shown dietary exposure among humans at 20%. Toxicological values from consumption of foodstuffs from canned foods and those of animal origin have been shown to increase health risks in humans, which include the reproductive system, mammary glands, metabolism, brain behavior, and heart health[13]. Regulations on the extensive BPA manufacturing or sale of products containing BPA have not been implemented in most countries despite the knowledge of its toxicity. This is due to the scientific evidence conflicting with direct effects on human health from the exposure of the contaminate.

CHAPTER II

INTRODUCTION

Electrochemistry and Electrolytic Cells

Electrochemistry can be used to study the movement of electrons in a chemical process. The movement of electrons occurs through oxidation-reduction reactions, or redox reactions, which are reactions involving an element's change in oxidation state by either gaining or losing an electron. Oxidation occurs with the loss of an electron, thus increasing the oxidation state, while a decrease in the oxidation state is observed through gaining an electron, known as reduction. Electrolytic cells undergo nonspontaneous reactions, requiring an external source of energy to drive a current through the system performing chemical reactions.

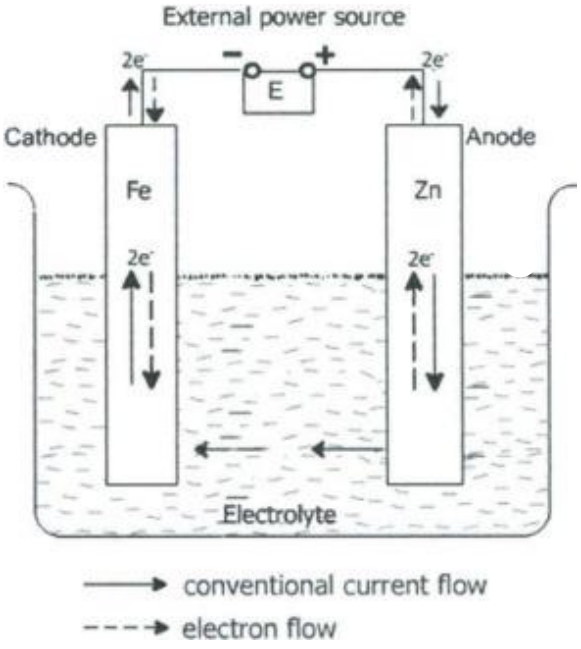

Figure 1: Electrolytic chemical cell setup[34].

The electrolytic cells consist of two half-cells, an oxidation half-cell, and a reduction half-cell, with the oxidation half-reaction occurring at the anode and the oxidation half-reaction occurring at the cathode. Both electrodes are submerged into an electrolyte solution, with the electron supply coming from the external source, and electron transfer occurring from one electrode to the other.

Graphene Oxide Structure and Properties

Graphene oxide, a member of the carbon materials family, is a two-dimensional sheet of carbon atoms that are sp^2 hybridized. The carbon atoms are packed in a hexagonal lattice. The structure can stack the sheets together creating membranes, as well as anchoring metal ions to the oxygen containing functional groups to generate composite materials. The thin carbon layer, 0.34nm, is lightweight, yet maintains a tensile strength of 130 GPa[15]. The nanosheets also contain great thermal and electrical conductivity properties. Due to the material's great properties of heat and electrical conduction, graphene oxide has been widely applied towards environmentally related interests.

NiS and CoS Structure and Properties

NiS and CoS nanocomposites obtain various interfaces and unique structures, both qualities which have been shown to perform efficiently as electrocatalysts, as well as exhibiting stability over long periods of time. The synergistic effect between the atoms allows for rapid electron transfer during the process of electrolysis. Nickel sulfides and cobalt sulfides both contain transition metals that are cost effective and found abundantly in nature.

NiS has been widely applied as an electrocatalyst due to its electrical, optical, and magnetic properties aiding in the ability to store energy. Its contrasting phases of the

rhombohedral structure, β-NiS, and metallic hexagonal structure, α-NiS, are highly crystalline in nature and both remain stable at various temperatures. NiS and its diverse, sulfur rich, arrangements display strong electrical conductivity, high surface area and morphology[17].

CoS has many applications in catalytic technology due to its supreme electrochemical energy storage and conversion, owing to its superb redox properties and high stability.

Kinetics

Kinetics studies provide information on chemical reactions over time due to concentration rates changing as reactants form products, until equilibrium has been achieved. The reaction dynamics are interpreted by examining the rate of the system and the contingency of the rate on the parameters of the system, or the number of phases in which the reaction occurs. The reaction rate will be found by the BPA concentration from the kinetics of degradation of BPA by the composite materials.

CHAPTER III

MATERIALS AND METHODS

Synthesis of Graphene Oxide (GO)

Graphene oxide was synthesized from graphite powder using a modified Hummers' Method (Flores et al., 2020). In brief combination of 3.0 g graphite flakes, 1.5 g $NaNO_3$, and 69mL H_2SO_4 was homogenized in a 500 mL round bottom flask fitted with a magnetic stir bar and then cooled to 4˚C. After cooling, 9.0 g $KMnO_4$ was gradually added, ensuring the temperature did not surpass 10˚C. The subsequent solution was heated and held between 35-40˚C for a duration of 30 minutes. After the 30-minute heating time 138 mL of 18 MΩ H_2O was added, dropwise, to prevent the temperature from increasing above 40˚C. After addition of the water the resulting mixture was heated to reaching 100˚C and held at temperature for 15 minutes and subsequently cooled to room temperature. After cooling an additional 420 mL 18 MΩ H_2O containing 3 mL of 30% H_2O_2 was added to the solution. GO particles were collected using vacuum filtration and washed with several portions of 18 MΩ H_2O followed by C_3H_6O, then oven dried at 85˚C overnight.

Synthesis of Expanded GO

The synthesized graphene oxide particles were placed in a porcelain ceramic boat inside of a Thermolyne tube furnace. The tube was purged with nitrogen gas for 20 minutes to remove the presence of air. Under a continuous flow of nitrogen gas, the sample was heated to 350˚C and

held at temperature for one hour. The sample was then cooled to room temperature naturally. All standards and samples underwent the same process for expansion.

Synthesis of Expanded NiS/GO Composite

In a 50 mL Eppendorf tube, a combination of GO, 19.8% $Ni(NO_3)_2$•$6H_2O$ (10 wt.% GO−Ni), and 98+% Na_2S•$9H_2O$ (10 wt.% GO−S) were homogenized in 18 MΩ H_2O and sonicated for 2 hours. The resulting mixture was filtered using vacuum filtration and washed using several portions of 18 MΩ H_2O and acetone which were subsequently vacuum dried overnight. The following particles were then heat treated in a Thermolyne tube furnace as previously described.

Synthesis of Expanded CoS/GO Composite

A combination of GO, $CoCl_2$•$6H_2O$ (10 wt.% GO−Co), and 98+% Na_2S•$9H_2O$ (10 wt.% GO−S) were homogenized in 18 MΩ H_2O in a 50 mL Eppendorf tube and placed in a sonicator for a period of 2 hours. The subsequent mixture was filtered via vacuum filtration and washed with several portions of 18 MΩ H_2O and C_3H_6O, and subsequently placed in a desiccator overnight. The resulting dried powder was accumulated in a loosely sealed vile inside of a desiccator overnight. The following particles were then heat treated in a Thermolyne tube furnace as previously mentioned.

Electrode Preparation

In a 50 mL Eppendorf tube, a combination of 10mg of catalyst was suspended in 1.25 mL 18 MΩ H_2O. To the mixture 50 μL 5% Naifon solution was added, and the mixture was sonicated for 1 hour generating electrolytic ink. The electrode support material, Cu foam, was cut to size, 1.5 * 3.0 cm^2, and washed using acetone (C_3H_6O). The Cu foam was in acetone was sonicated for 30 minutes, dried, and subsequently submerged in 0.1M HCl for 30 seconds and

washed with 18 MΩ H_2O and dried again. A 300 μL aliquot of electrolytic ink was applied to the support material and air dried overnight. Additionally, the electrode was dried in an oven at 80˚C for 2 hours.

Electrolytic Cell Setup

The constructed electrolytic cell setup consisted of an external power source with the positive terminal connected to a titanium electrode and the negative terminal connected to the fabricated Cu-composite electrode. Both electrodes were submerged in a 400 mL Pyrex beaker fitted with a magnetic stirrer, containing 250 mL 30ppm 97+% $C_{15}H_{16}O_2$ in Na_2SO_4 electrolyte solution at room temperature. Electrolysis trials were performed with altered parameters, which included different quantities of added electrolyte NaCl, of 1.0 g/L, 2.0 g/L, and 4.0 g/L, different pH levels, 2, 4, and 6, and constant current conditions applied at either 0.100 A or 0.200 A to determine the optimum degradation conditions. Samples of each trail were taken before current was applied, 30 minutes and 60 minutes after to observe BPA degradation over time.

Characterization

Characterization of the expanded graphene oxide expanded NiS/GO composites and expanded CoS/GO composites were performed using x-ray diffraction (XRD) and scanning electron microscopy (SEM) prior to performing the degradative studies. Samples taken before, during and at the completion of the degradative trials were examined using high pressure liquid chromatography (HPLC) and liquid chromatography-mass spectrometry (LC-MS).

XRD Analysis

A Bruker D2 Phaser Diffractometer was used to perform the XRD data collection. The XRD was equipped with a cobalt x-ray source and an iron filter, the diffractometer radiation

generated was 1.789 Å. The data was collected using the following parameters 5 seconds per step in increments of 0.02° and a range in 2θ ranging from 5-80° and the data analysis was performed using the LeBail fitting procedure in the Fullprof software and crystallographic data from the literature values[21-36].

SEM Analysis

A Zeiss EVO LS 10 scanning electron microscope was utilized to capture SEM images. Under a voltage of 10.94 kV and working distance of 29 to 39 mm, electron micrographs were obtained.

HPLC Analysis

The high-pressure liquid chromatography (HPLC) analysis of the standard and sample solutions was performed on a Dionex UltiMate 3000 system, consisting of a pump (LPG-3400SD), column oven (TCC-3000), and UV detector (DAD-3000). The analytical column was a HyPURITY C18 (15cm * 4.6 mm), with a particle size of 3 μm (ThermoFisher). The mobile phase consisted of water-acetonitrile (60:40, v/v)[39], at a flow rate of 0.500 mL/min with a total run time of 15.00 minutes. Each sample consisted of a 20 μL volume of injection with scans collected at a UV wavelength of 228 nm.

LCMS Analysis

An Agilent Technologies 6420 Triple Quad LC/MS was used for analysis, using a modified method similar to Jurek and Leitner (2018). The mobile phase consisted of LC-MS grade methanol and ultrapure water with a flow rate of 1.0 mL/min. The gradient conditions were 35% methanol at the beginning and then linearly increased to 100% in 10 minutes. H_2O started at 65% at the beginning and then linearly decreased to 0% in 8 minutes. MS/MS

acquisition was operated using the negative-ion mode with the capillary voltage at -3.5 kV. The gas flow was increased to 8.00 L/min, while the binary pump flow was set to 1.00 mL/min. Both the reaction and control were analyzed[18].

Degradation Studies

Degradation studies utilized electrolysis performed with a MDC01 DC Power Supply as the external energy source. The circuit was completed with a titanium anode, pure GO, NiS/GO or CoS/GO composite supported on a Cu cathode, and reaction solution containing Na_2SO_4 electrolyte containing and a 30ppm BPA concentration. The reactions were performed using constant agitation using a magnetic stir bar. All studies were performed in triplicates for each altered parameter to ensure reproducibility and affirmation of data.

pH Study

pH levels ranging between 2 and 6 were used to study the effectiveness of the catalysts in BPA degradation. For the pH studies a 250 mL solution of 30ppm 97+% $C_{15}H_{16}O_2$ (BPA) in a Na_2SO_4 electrolyte solution, at room temperature, and the reaction was performed in a 400 mL Pyrex beaker. pH adjustment was performed using either dilute NaOH or HCl. The reactions were studied for a duration of 1 hour, with aliquots collected before, and after the degradation study.

Kinetics Studies

The remaining concentration of BPA in the solution was recorded over the duration of 1 hour of degradation. For maximum efficiency, conditions of BPA solution, electrolyte concentration, pH, and current were applied. Reactions were executed in a 400mL Pyrex beaker

containing 250mL of 30ppm BPA solution. In 30 minute intervals, samples at a volume of 1mL were obtained.

Zero-order kinetics can be determined graphically by plotting reactant concentration versus time. Data resulting in a straight line indicates rate of reaction is not affected by species concentration. The slope of the line illustrates the negative of the rate constant and is defined by the zero-order integrated rate law equation:

$$[X] - [X_0] = -kt$$

Where k is the rate constant, t is time, $[X]$ is the concentration at any point in time and $[X_0]$ is the concentration when time is equal to zero. Plotting the natural log of the concentration versus time determines first-order kinetics. Data resulting in a straight line indicates rate of reaction is inversely affected by the species concentration. The slope of the line illustrates the negative of the rate constant and is defined by the first-order integrated rate law equation:

$$LN\left(\frac{[X]}{[X_0]}\right) = -kt$$

Plotting 1/ the concentration versus time determines second-order kinetics. Data resulting in a straight line indicates rate of reaction is directly affected by the species concentration. The slope of the line illustrates the positive rate constant and is defined by the second-order integrated rate law equation:

$$\frac{1}{[X]} - \frac{1}{[X_0]} = kt$$

Plots were produced from graphing the inverse of the remaining BPA concentration as a function of time, with the negative order corresponding to first-order kinetic reaction[20]

Electrolyte Study

The electrolyte was added at the following amounts 0.5 g Na_2SO_4 / 500 mL 18 MΩ H_2O, 1.0 g Na_2SO_4 / 500 mL 18 MΩ H_2O, and 2.0 g Na_2SO_4 / 500 mL 18 MΩ H_2O. The electrolyte was combined with 30ppm 97+% $C_{15}H_{16}O_2$ to determine the efficiency of the catalyst. 250 mL amounts of the individual solutions were placed in a 400 mL Pyrex beaker to be tested at room temperature. All fabricated electrodes were used for the degradation of BPA using each of the 3 solution mixtures.

Current / Potential Study

To determine the effectiveness of the catalyst under various conditions, each study was tested at an applied current of 0.100 A and 0.200 A, aiding in establishing the resulting potential. Varying the current allowed for the determination of the optimum reaction conditions.

CHAPTER IV

RESULTS AND DISCUSSION

XRD Results

Table 1: Fitted lattice parameters for all catalysts.

Fitted Lattice Parameters

Sample	**Phase**	**Space group**	**a(Å)**	**b(Å)**	**c(Å)**	**α(°)**	**β(°)**	**γ(°)**	**χ^2**
Graphite	Graphite	P63/mmc	2.43(1)	2.43(1)	6.69(4)	90.00	90.00	120.00	2.40
Graphene Oxide	Graphite	P63/mmc	2.43(1)	2.43(1)	18.09(2)	90.00	90.00	120.00	2.18
	GO	P63/mmc	2.43(1)	2.43(1)	6.69(4)	90.00	90.00	120.00	
Ni_xS_y-GO	NiS	R3M	9.59(5)	9.59(5)	3.20(5)	90.00	90.00	120.00	2.46
	Graphene	P63/mmc	2.43(1)	2.43(1)	6.69(4)	90.00	90.00	120.00	
	NiS	P63mmc	3.41(7)	3.41(7)	5.26(6)	90.00	90.00	120.00	
	Ni3S4	Fd3m	9.39(3)	9.39(3)	9.39(3)	90.00	90.00	90.00	
Co_xS_y-GO	CoS	P63/mmc	3.31(1)	3.31(1)	5.10(1)	90.00	90.00	120.00	1.69
	Graphene oxide	P63/mmc	2.43(1)	2.43(1)	6.69(4)	90.00	90.00	120.00	
	Co2S3	P31C	6.54(3)	6.54(3)	16.41(7)	90.00	90.00	120.00	

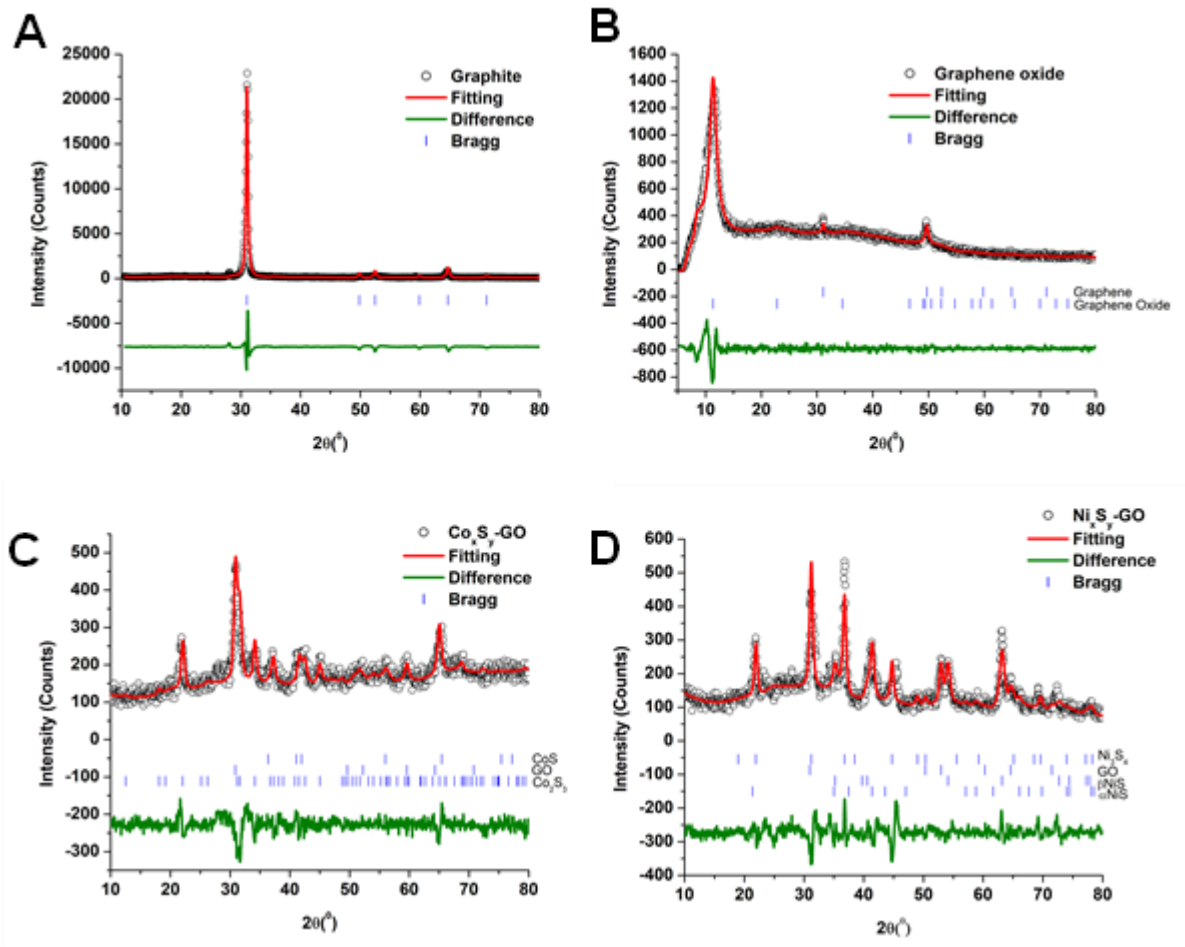

Figure 2: Le Bail fitting of the X-ray Powder diffraction of (A) graphite, (B) graphene oxide, (C) Co_XS_y-GO composite, and (D) Ni_xS_y- GO composite electrocatalytic materials.

For all catalysts, powder X-ray diffraction was used to achieve phase identification. X-ray diffraction fittings were generated by LeBail fitting procedures with Fullprof software. For all catalyst materials, literature values were utilized to acquire crystallographic data.

Figure 2 shows the X-ray powder diffraction pattern of the different materials used to make the electrodes. Graphite was the initial starting material, which was modified and

converted into graphene oxides. Figure 2A shows the diffraction pattern and the Le Bail fitting of initial starting material graphite, which is the standard diffraction pattern observed for graphite in the literature. From the fitting the lattice was determined to be hexagonal (p63/mmc), with the lattice parameters given in Table 1 the reduced $\chi 2$ for the fitting was 2.40, which indicated a good fitting. The Le Bail fitting reduces the $\chi 2$ to 1, the closer the value is to 1 the better agreement between the data and the literature values. A Le Bail fitting below 5 is considered a great fitting. The diffraction pattern show a large diffraction peak located at 30.92° in 2θ, which represents the 002 diffraction plane for graphite. The 002-diffraction plane in graphite represents the c-axis of the crystal, which indicates the plane stacking observed (Figure 2). Figure 2B shows the diffraction pattern of GO, which is characteristic of the diffraction patterns observed in the literature for graphene oxide. However, due to the variability of the structure of graphene oxide no absolute accepted crystal structure is known for GO. From the fitting the GO was determined to be a combination of GO and graphite the reduced χ^2 for the fitting was 2.18 which indicates a good agreement between the data and the literature values. The peak observed at 11.36° is the 002 plane for GO, which represents the c-axis and represents the number of places stacked together. In fact the 002 plane of GO and graphite are the same plane, the shift in the position of the 002 after oxidation of the graphite is caused by an expansion of the lattice along the C-axis. The shift in the C-axis is from 6.69 to 18.09 Å the axis is almost tripled of the C-axis, a representation of this is show in Figure 2. The shift in the c-axis changes in the interlayer space from 3.38 Å to 8.87 Å as shown in Figure 2. In addition, in the GO there is a small amount of non-oxidized graphite present, as was indicated by the diffraction peak located at 30.92° in 2θ. Figure 2C shows the diffraction pattern of the Co_xS_y graphene oxide composite material. The sample was determined to consist of three phases, which were graphite (or

graphene), hexagonal CoS and Co_2S_3. The fitting showed a reduced χ^2 of 1.69, indicating a good agreement between the data and the literature. The final Figure 2D shows the Ni_xS_y-GO diffraction pattern and Le Bail fitting, which indicate the presence of 4 phases in the sample. The observed phases in the sample were Ni3S4, α-NiS, β-NiS, and graphite (graphene). All the lattice parameters are shown in Table 1 and are within reason with the literature. The reduced χ^2 for the fitting was 2.46 indicating a good agreement between the data and the literature. The presence of graphene and not graphene oxide could mean one of two things. First there may have been a reduction of the graphene oxide to generate reduced graphene oxide (rGO) which has a diffraction pattern similar to graphene; alternatively, or second the graphene oxide may have completely exfoliated into individual sheets and only the small layers of graphene are visible in the X-ray diffraction. A small amount of graphite/graphene is visible in the diffraction pattern of the graphene oxide (Figure 2B).

Kinetic Studies Results

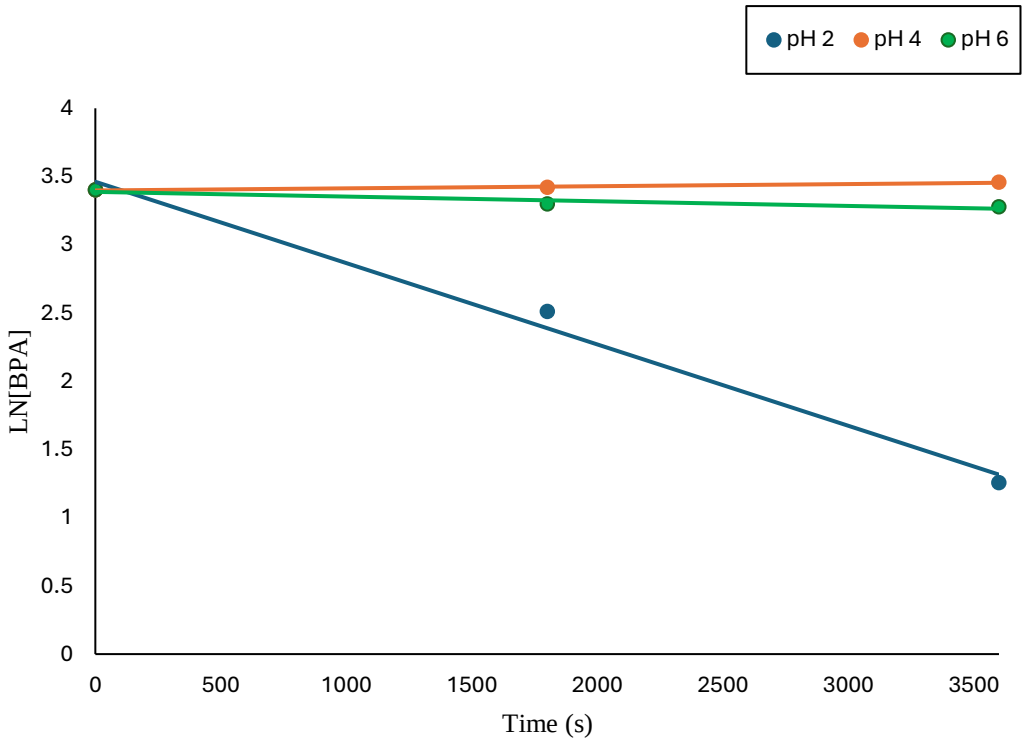

Figure 3: Kinetic plot for NiS/GO composite at pH 2, 4 and 6.

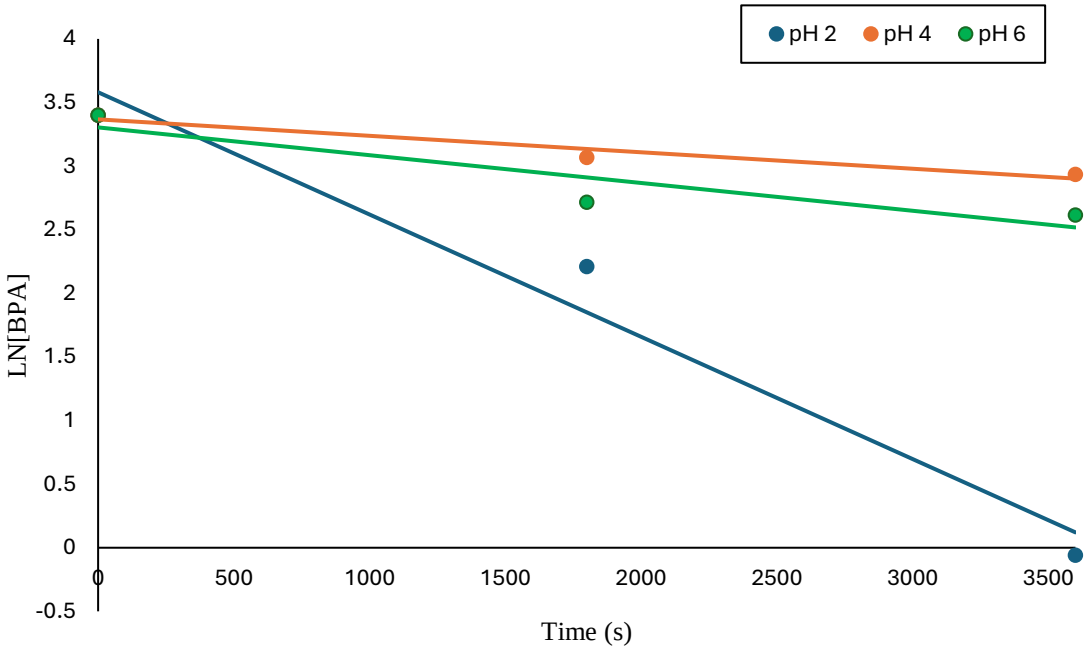

Figure 4: Kinetic plot for CoS/GO composite at pH 2, 4 and 6.

The natural logarithm of the remaining BPA concentration in solution was plotted as a function of time to represent the catalytic degradation of NiS/GO, shown in Figure 3, and of CoS/GO shown in Figure3. For each catalyst, the results are plotted over a 1-hour cycle period. For each of the reactions, the slope of the individual lines demonstrated is equal to the rate constant, expressed as s^{-1}. The rate of BPA degradation via the NiS/GO composite had the highest magnitude at pH 2 (-0.0006 s^{-1}), followed by pH 6 (-3.00 X 10^{-05} s^{-1}) and then pH 4 (2.00 X 10^{-05} s^{-1}). The reaction rate at pH 2 far surpass the rate associated at pH 4 and pH 6 for the NiS/GO composite. The rate of BPA degradation via the CoS/GO composite also expressed the highest magnitude at pH 2 (-0.001 s^{-1}), followed by pH 6 (-0.0002 s^{-1}) and then pH 4 (-0.0001 s^{-1}). Similar to the NiS/GO composite, the reaction rate for the CoS/GO composite at pH 2 far surpass the rate associated at pH 4 and pH 6.

All processes of BPA decomposition by both NiS/GO and CoS/GO composites proceeded as a 1st order reaction. The linear relationship depicted by experimental data in Figures 3 and 4 when plotting the natural logarithm of the remaining BPA concentration versus time in seconds over a 1-hour cycle justifies the 1st order reaction.

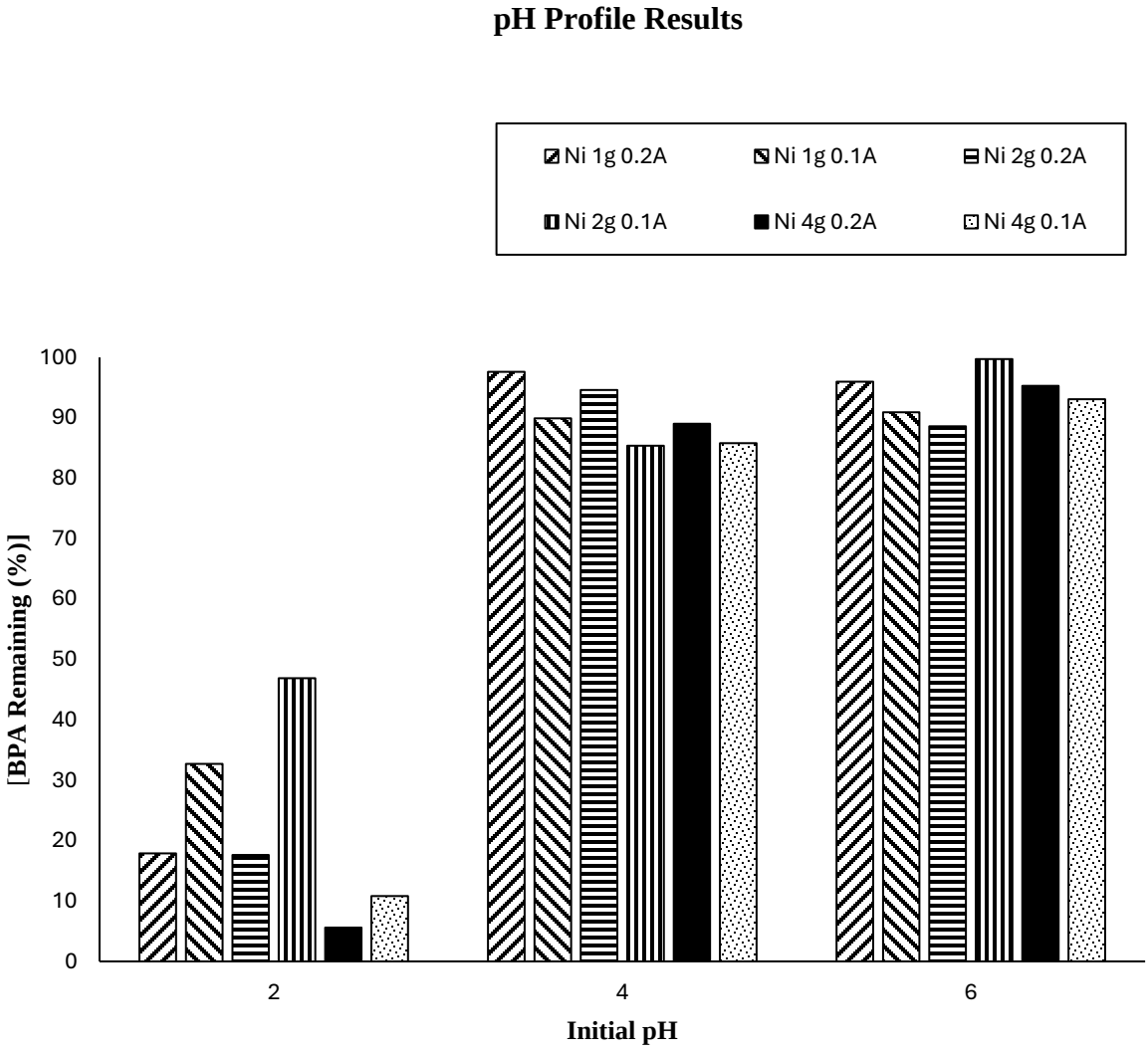

Figure 5: Effects of initial pH on the catalytic efficiency of NiS/GO composites.

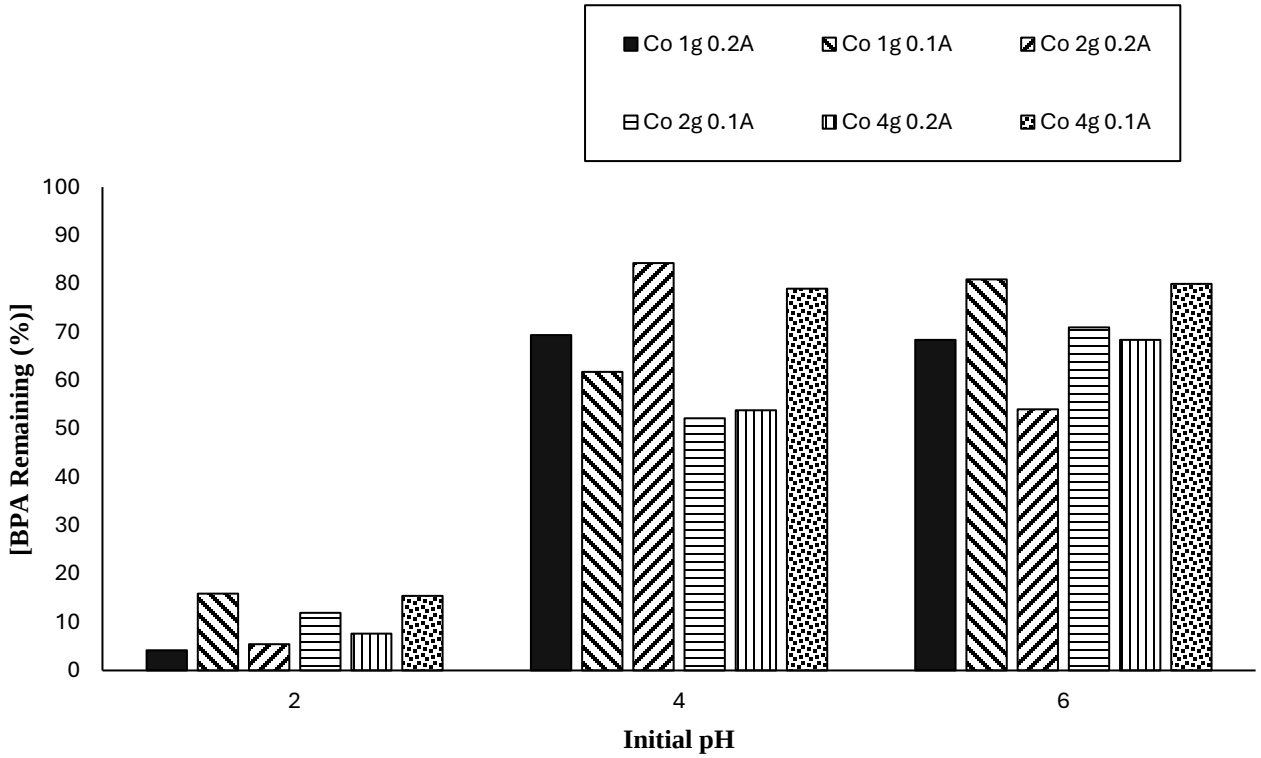

Figure 6: Effects of initial pH on the catalytic efficiency of CoS/GO composites.

The efficiency of the catalyst for both the NiS/GO and CoS/GO composites were analyzed at a pH of 2, 4, and 6. The results for the NiS/GO composites are shown in Figure 5, and Figure 6 displays the CoS/GO composite results. The catalytic efficiency is established by the percent concentration of BPA degraded over a 1-hour period of degradation, from the initial 30ppm BPA present in the electrolyte solution. Both composite catalysts previously mentioned, show maximum capability to degrade BPA at a pH of 2. At this pH, 82.1% of BPA was degraded by the NiS/GO composite containing 1.0g/L Na_2SO_4 electrolyte in solution at 0.2A, 67.3% by the composite at 0.1A, 82.4% for the composite with 2.0g electrolyte at 0.2A and 53.1% at 0.1A, 94.4% for the composite with 4.0g electrolyte at 0.2A and 89.2% at 0.1A. Similarly at this pH, 95.8% of BPA was degraded by the CoS/GO composite containing 1.0g/L Na_2SO_4 electrolyte in

solution at 0.2A, 84.1% by the composite at 0.1A, 94.6% for the composite with 2.0g electrolyte at 0.2A and 88.1% at 0.1A, 92.4% for the composite with 4.0g electrolyte at 0.2A and 84.6% at 0.1A. As the pH increased, both composites encountered a decrease in the efficiency of the catalyst. The highest concentration of BPA degraded at pH 4 for any of the NiS/GO composites was 14.6% at a current of 0.1A and 2.0g electrolyte, and 47.8% degraded at a current of 0.1A and 2.0g electrolyte for any of the CoS/GO composites. At a pH of 6, the largest BPA degradation percentage for the NiS/Go composites was 11.4% at a current of 0.2A and 2.0g electrolyte, and only 46% for the CoS/GO composites at 0.2A and 2.0g.

The solubility of BPA in solution as displayed immensely decreased with an increase in pH. The kinetics of BPA degradation by both composites depicted a direct dependence on BPA concentration by the reaction rate, thus the optimal pH for degradation should be fixed at 2.

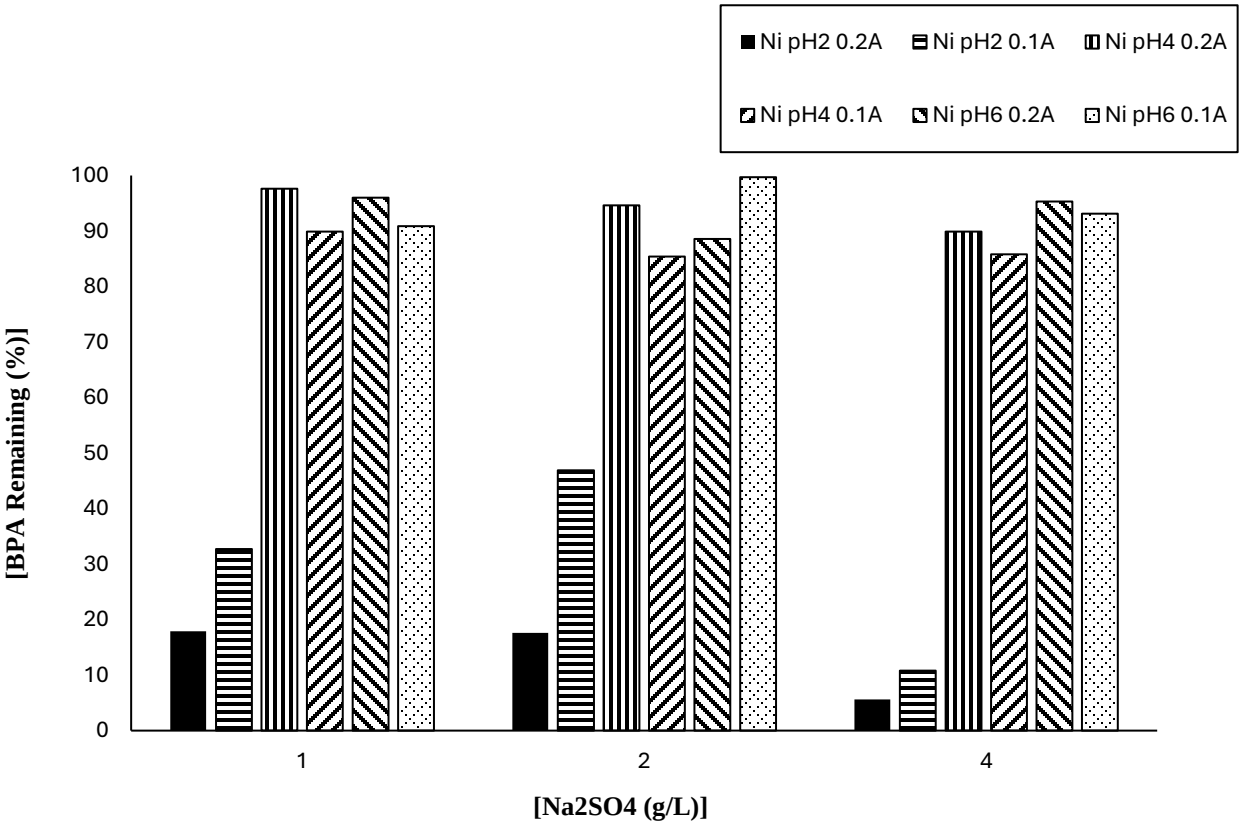

Figure 7: Effects of electrolyte concentration, [Na_2SO_4], on the catalytic efficiency of NiS/GO composites.

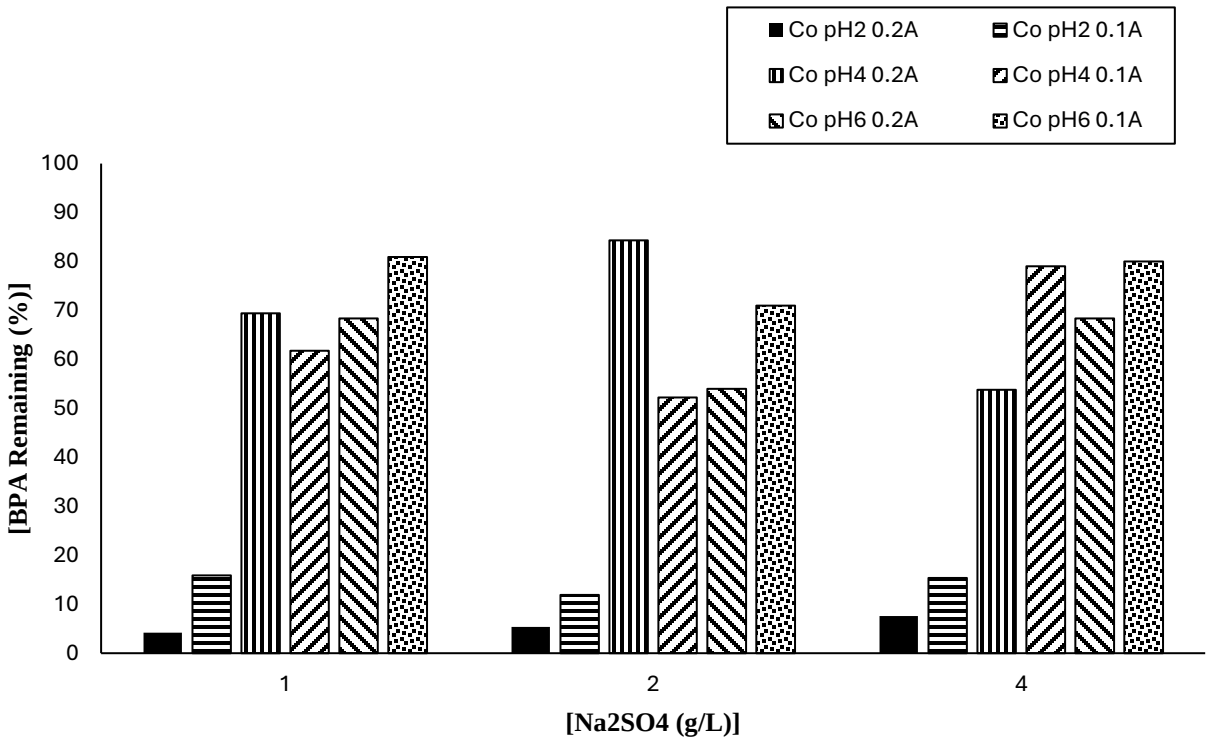

Figure 8: Effects of electrolyte concentration, [Na_2SO_4], on the catalytic efficiency of CoS/GO composites.

The catalytic efficiency of the composites, NiS/GO and CoS/GO, were tested with varying electrolyte concentrations of 1.0 g/L, 2.0 g/L, and 4.0 g/L Na_2SO_4, with the results displayed in figures 7 and 8. The catalytic efficiency was based on the percent concentration of BPA degradation during a cycle of 1-hour. A significant difference in BPA solubility was not established by increasing the electrolyte concentration in solution for both composite materials. The highest concentration of BPA degraded occurred with 1.0 g/L, 2.0 g/L, and 4.0 g/L Na_2SO_4 at 82.1%, 82.4%, and 94.4%, respectively for the NiS/GO composite, and 95.8%, 94.6%, and 92.4%, respectively for the CoS/GO composite, with both composites under conditions of a pH of 2 and current of 0.2A. Similarly at a pH of 2 and applied current of 0.1A, BPA solubility was

adequate at all concentrations of electrolyte for both composites; 67.3%, 53.1%, and 89.2% respectively for NiS/GO and 84.1%, 88.1%, and 84.6% respectively for CoS/GO. Any other conditions applied at each of the 3 different electrolyte concentrations minimal solubility of BPA was observed.

BPA degradation coupled with increasing concentrations of Na_2SO_4 in solution, had no distinct influence. Consequently, there was no optimal concentration of the electrolyte for the efficiency of the catalysts.

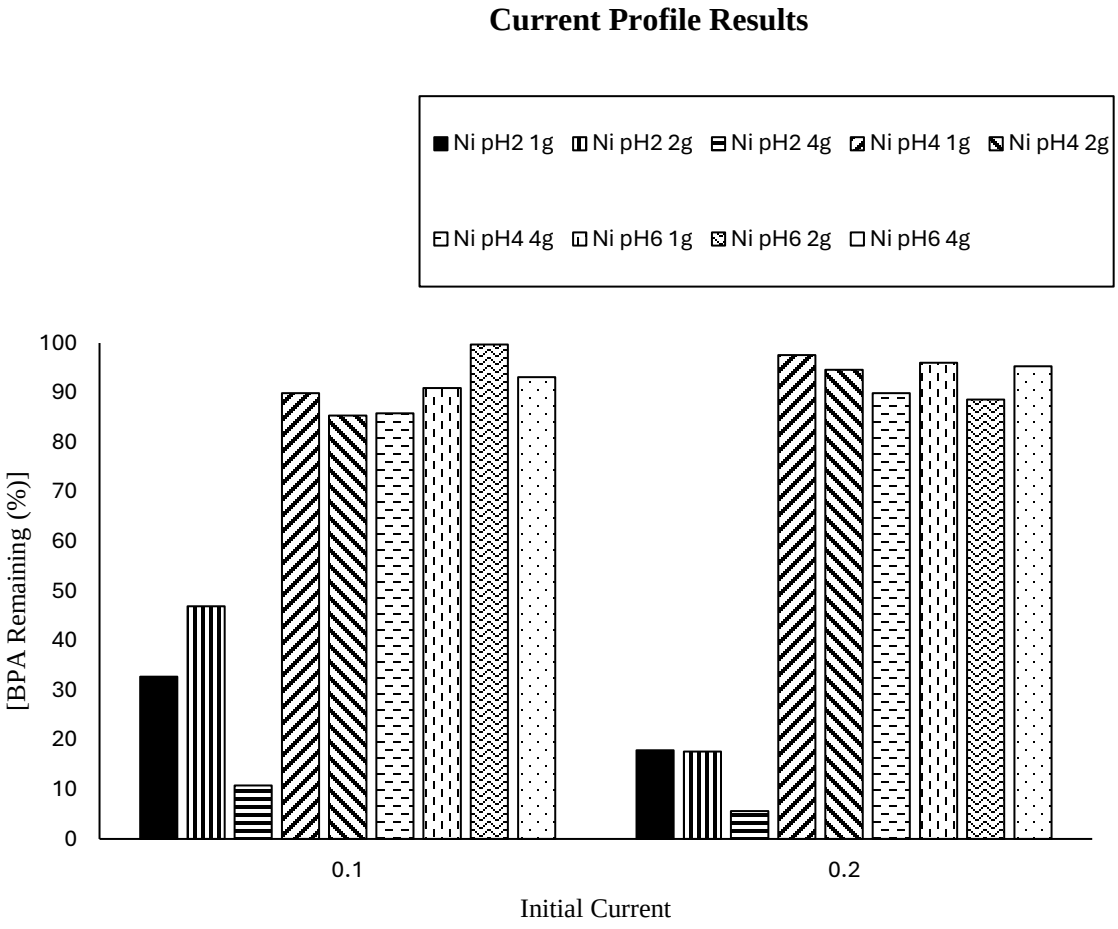

Figure 9: Effects of current on the catalytic efficiency of NiS/GO composites.

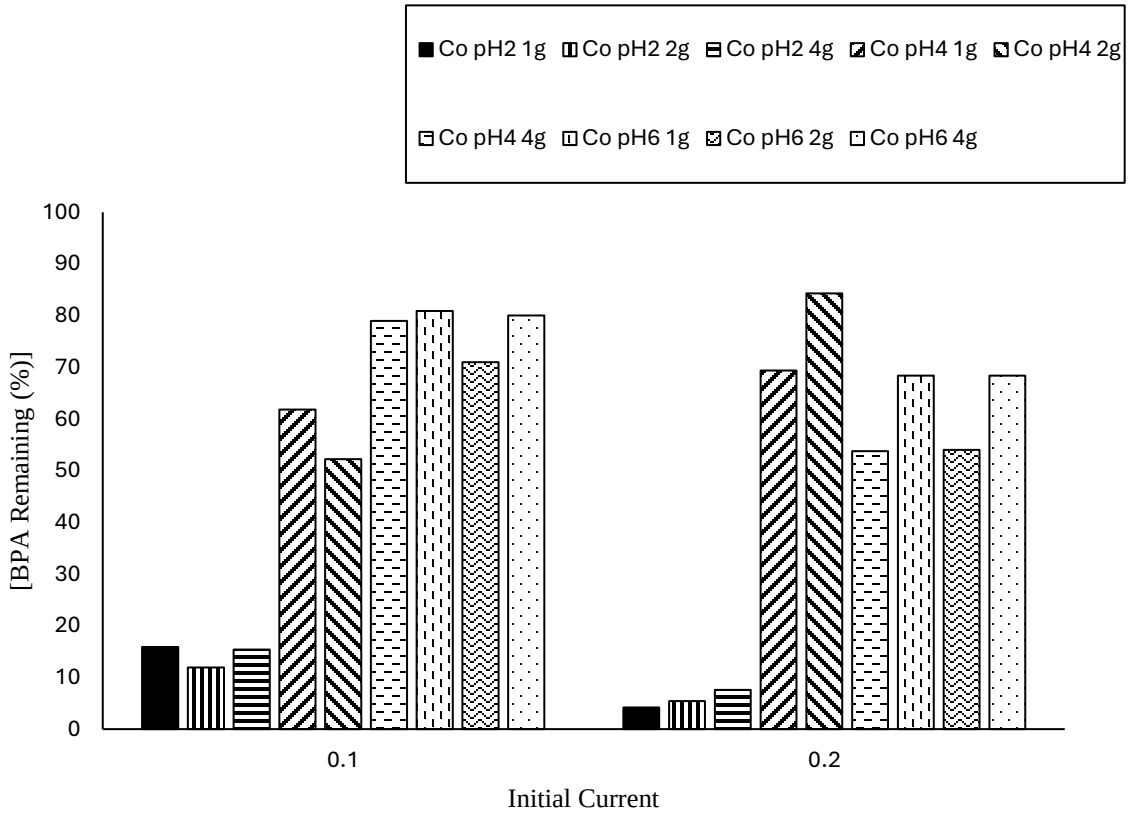

Figure 10: Effects of current on the catalytic efficiency of CoS/GO composites.

Figures 9 and 10 display the data from the varying currents applied to the system for both NiS/GO and CoS/GO catalysts and the correlated percentage of BPA solubility over a 1-hour degradation cycle. Constant currents of 0.100 A and 0.200 A were tested to determine the effect, if any, on the catalysts. For both, the opposing constant current conditions did not prove a severe distinction in BPA solubility. In both cases, at a pH of 2, the applied current degraded larger than 50% of the pollutant. For the nickel containing composite at pH2, with 1.0g electrolyte 67.3% was degraded with 0.1 A and 82.1% solubility at 0.2A, 53.1% solubility at 0.1A and 82.4% at 0.2A with 2.0g electrolyte, and 89.2% BPA degradation at 0.1A and 94.4% at 0.2A with 4.0g electrolyte added.

For each of the studies occurring at pH 2, the higher current applied did reduce the BPA concentration more. With 1.0g electrolyte addition, 14.8% more degradation occurred at a current applied at 0.2A rather than 0.1A. Similarly, 29.3% more solubility was observed at the higher current with 2.0g electrolyte present, and 5.2% more at the higher current with 4.0g present. At pH 4, 0.1A current reduced the pollutant more, showing a percent concentration difference of 7.7%, 9.2% and 4.1% with increasing electrolyte addition. For conditions at a pH of 6, 5.1% more solubility occurred with the lower current and least amount of electrolyte added, while the higher current showed more reduction in concentration with increasing electrolyte amounts, differing by 11.1% and 2.2%.

Similar results can be seen in Figure 10 for the CoS/GO composite when an increasing current is applied to the system. For the cobalt containing composite at pH2, with 1.0g electrolyte 84.1% was degraded with 0.1 A and 95.8% solubility at 0.2A, 88.1% solubility at 0.1A and 94.6% at 0.2A with 2.0g electrolyte, and 84.6% BPA degradation at 0.1A and 92.4% at 0.2A with 4.0g electrolyte added. Under conditions of pH 2 and increasing electrolyte addition, the higher current applied showed a larger effect on the solubility of the pollutant.

In 2 of the 3 cases at pH 2 and a current of 0.2A, the cobalt containing catalyst did ensure removal of BPA from the water more so than that of the nickel containing composite. With the addition of 1.0g electrolyte, CoS/GO reduced the concentration by 13.7% more than when using NiS/GO and 12.2% more with 2.0g. With the addition of 4.0g electrolyte at pH2, the nickel composite reduced the pollutant by only 2.0% more than that containing cobalt, at the higher current.

For conditions at pH 4, the lower current reduced BPA concentration more with 1.0 and 2.0g electrolyte at 7.6% and 32.1%, respectively, with 25.2% more degradation at 0.2A and 4.0g. For each case at pH 6, the higher current applied decreased concentration more with increasing electrolyte addition at 12.5%, 17.0% and 11.6%. The higher current proved to have a larger effect on all but 3 tests using the CoS/GO catalyst.

In most, but not all cases for both the NiS/GO and CoS/GO composites, the larger current applied to the system tended to remove more of the pollutant from the system, therefore it cannot be confirmed that the application of increasing current is optimal for catalytic efficiency.

Under all altered conditions, aside from one, the presence of the CoS/GO composite had a larger reductive effect on the concentration of BPA remaining in solution as compared to the presence of NiS/GO as the catalyst. The only case in which the NiS/GO composite proved to work better is at pH 2, an applied current of 0.2A and 4.0g of electrolyte added to solution, with only 2% more reduction in BPA concentration observed. With the experimental data, it can be determined that the optimal composite for catalytic efficiency in this study is CoS/GO.

SEM Results

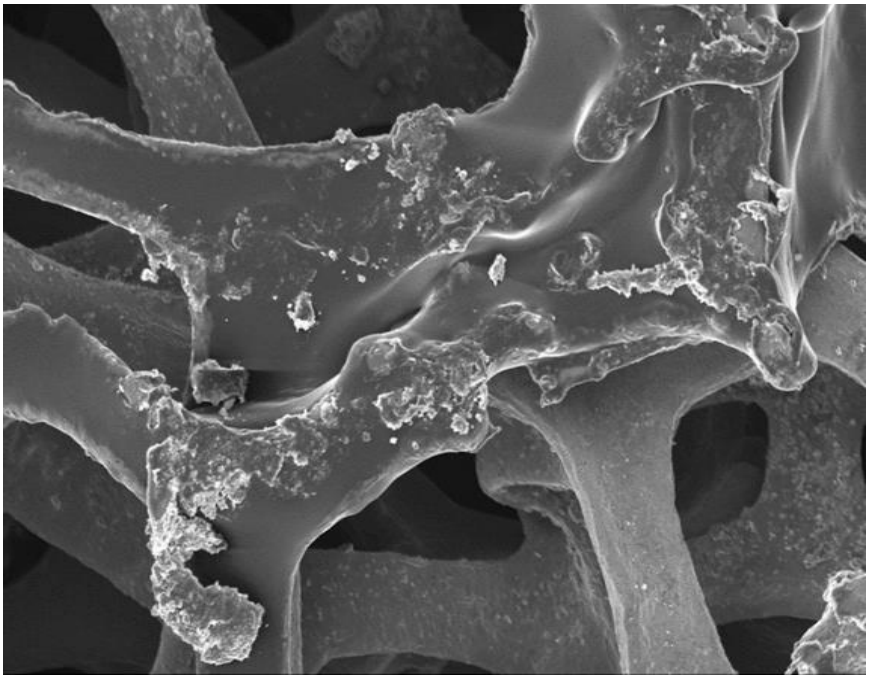

Figure 11: SEM image of unused NiS/GO cathode.

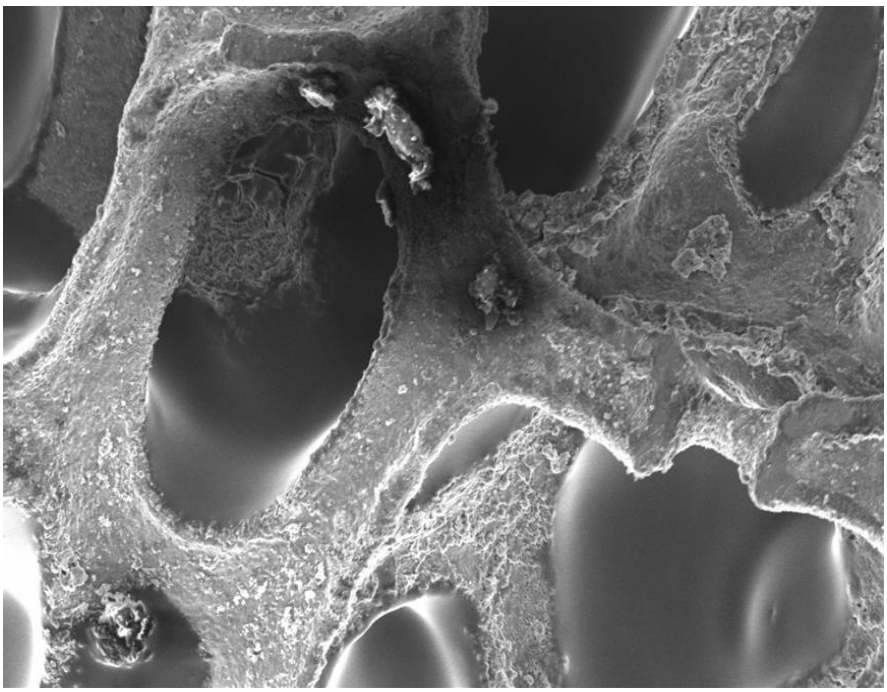

Figure 12: SEM image of NiS/GO cathode at pH2 and 0.1A with 0.5g electrolyte after 60 minutes.

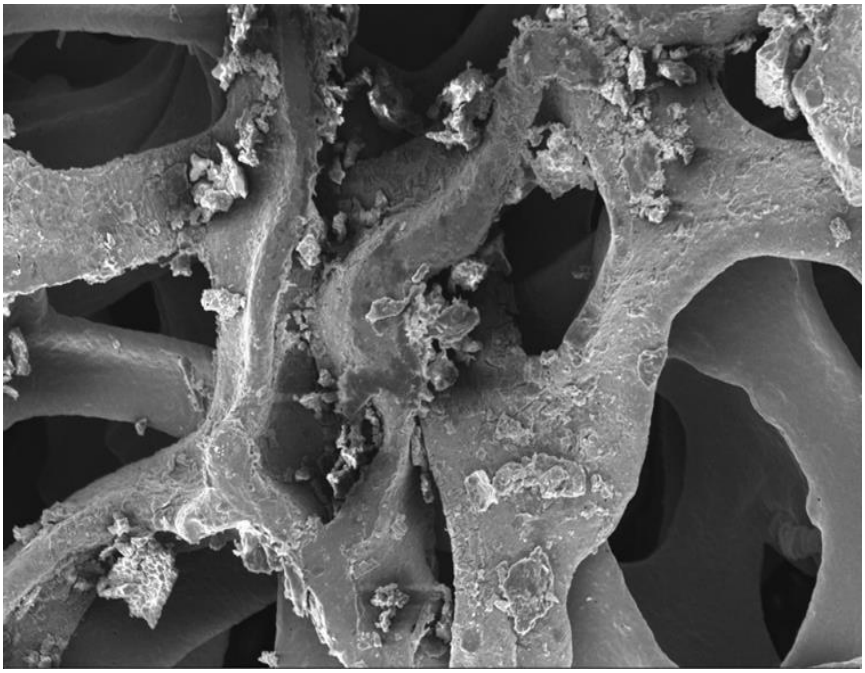

Figure 13: SEM image of unused CoS/GO cathode.

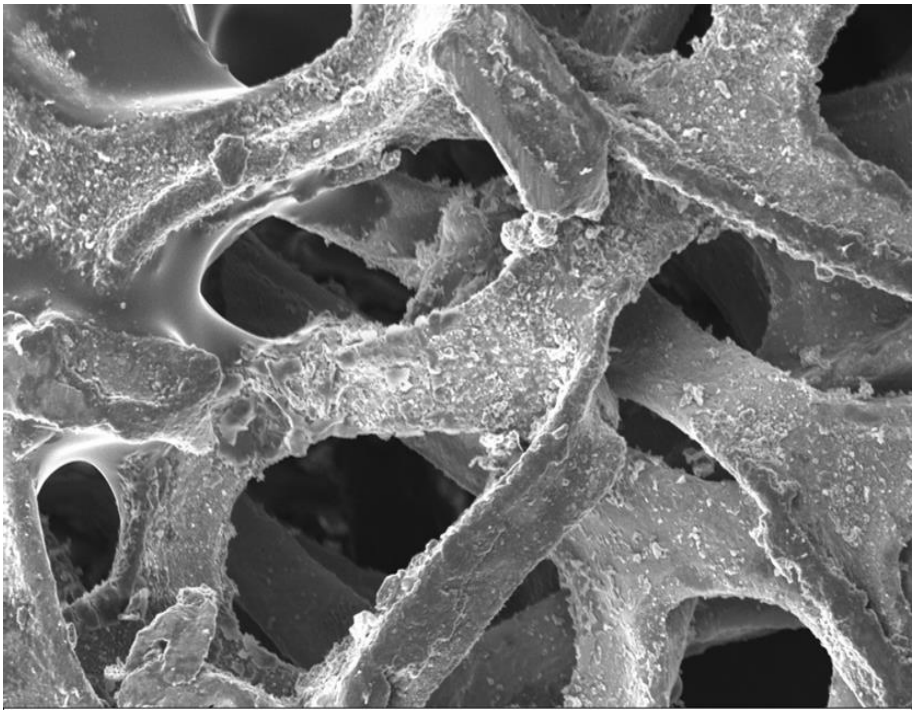

Figure 14: SEM image of CoS/GO cathode at pH2 and 0.1A with 0.5g electrolyte after 60 minutes.

A scanning electron microscope was utilized to capture SEM images. Under a voltage of 10.94 kV and working distance of 29 to 39 mm, electron micrographs were obtained. Figures 11 and 13 show the SEM images of unused NiS/GO and CoS/GO cathodes. Figures 12 and 14 are the captures SEM images of NiS/GO and CoS/GO cathodes, both at pH2 and 0.1A with 0.5g electrolyte after a 1-hour degradation cycle. It is evident in the comparison between the unused cathodes and cathodes that underwent the degradation period, that the composite is much rougher on the surface. This may be attributed to the attaching of BPA particles on the composite cathodes, as they appear to be uniformly covered[19].

LCMS Results

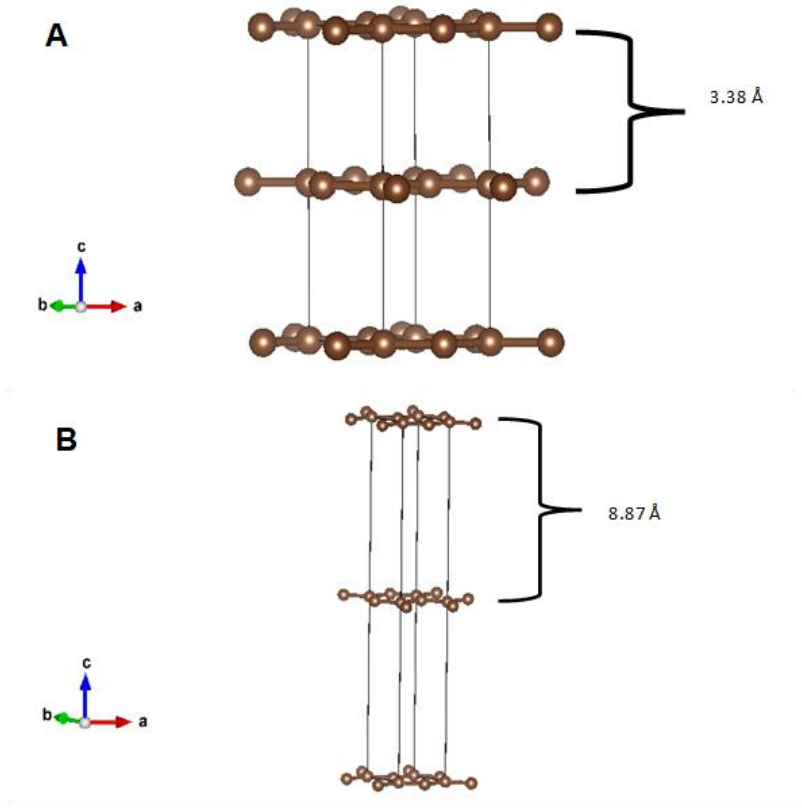

Figure 15: Representation of the layered structure of graphite (A) and graphene oxide (B).

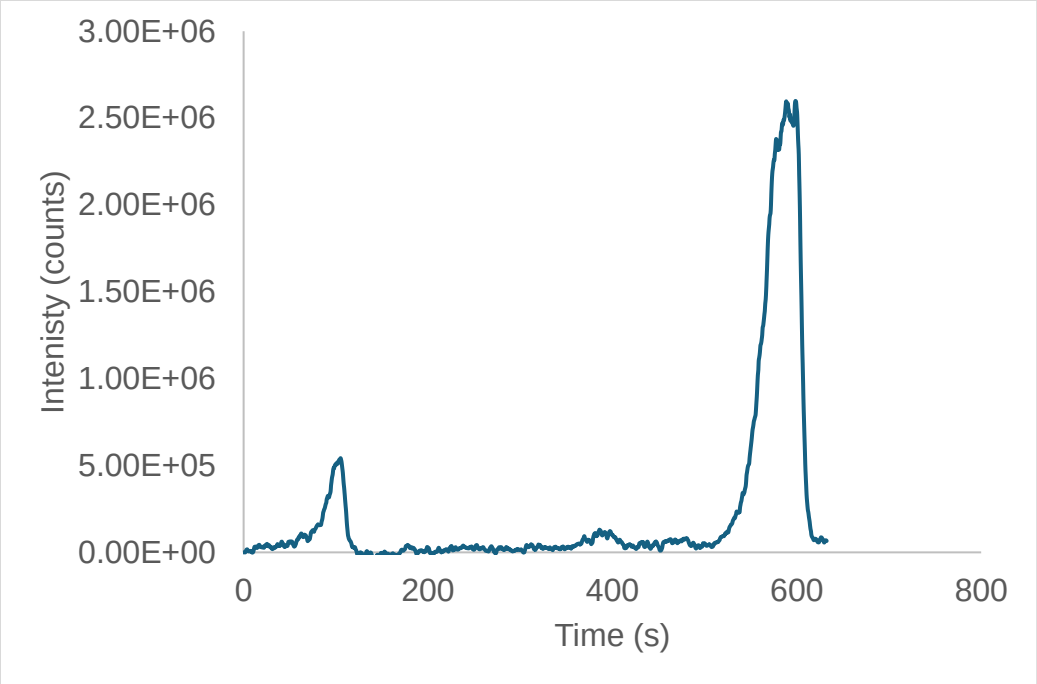

Figure 16: LC-MS chromatogram of the BPA starting material.

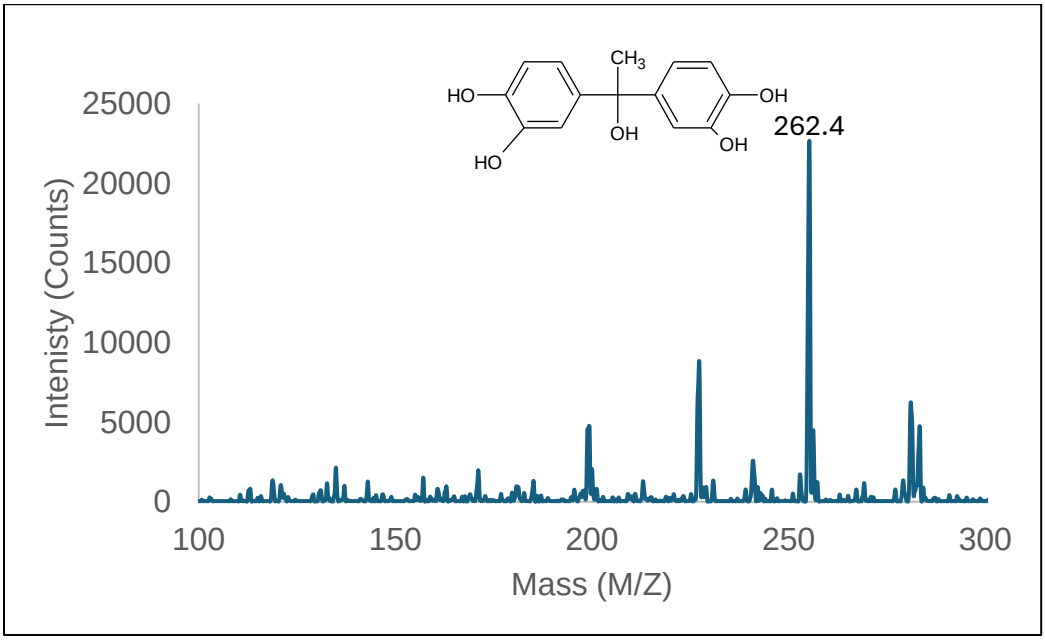

Figure 17: MS spectra of compound in peak retained at 101s.

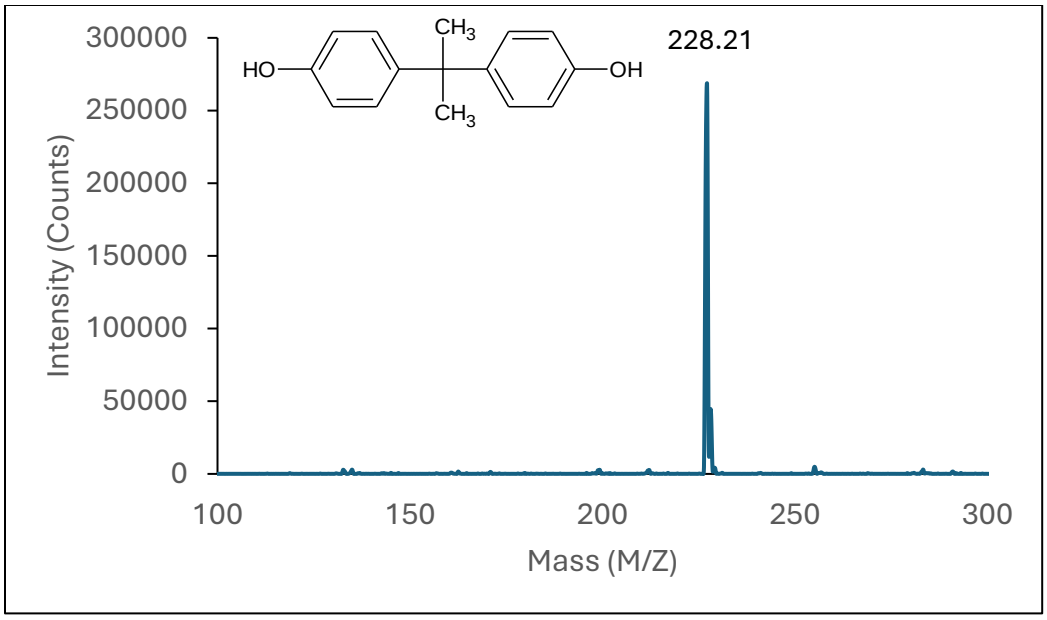

Figure 18: LC-MS mass spectra compound related at 589s bisphenol A.

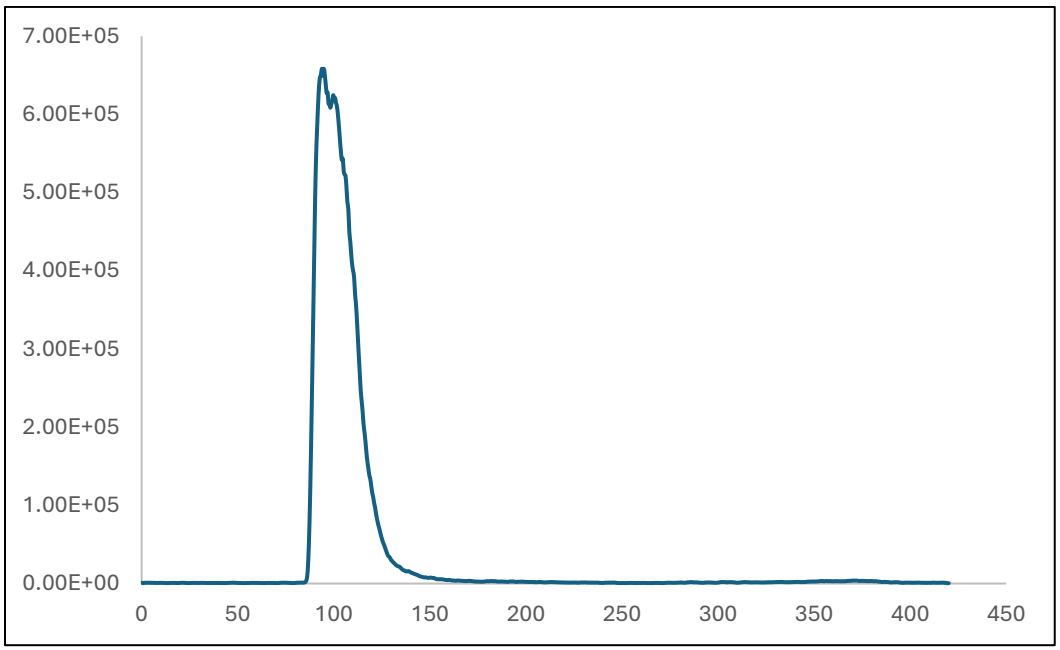

Figure 19: LC-MS chromatogram of solution after electrocatalytic reaction.

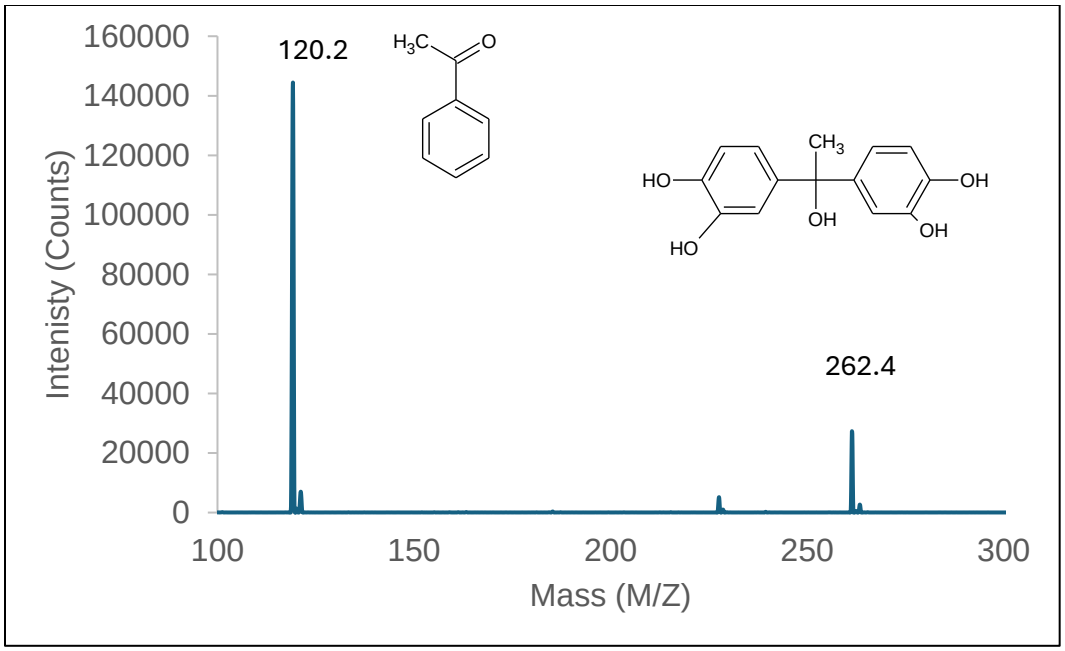

Figure 20: LC-MS of reaction compounds after CoS.

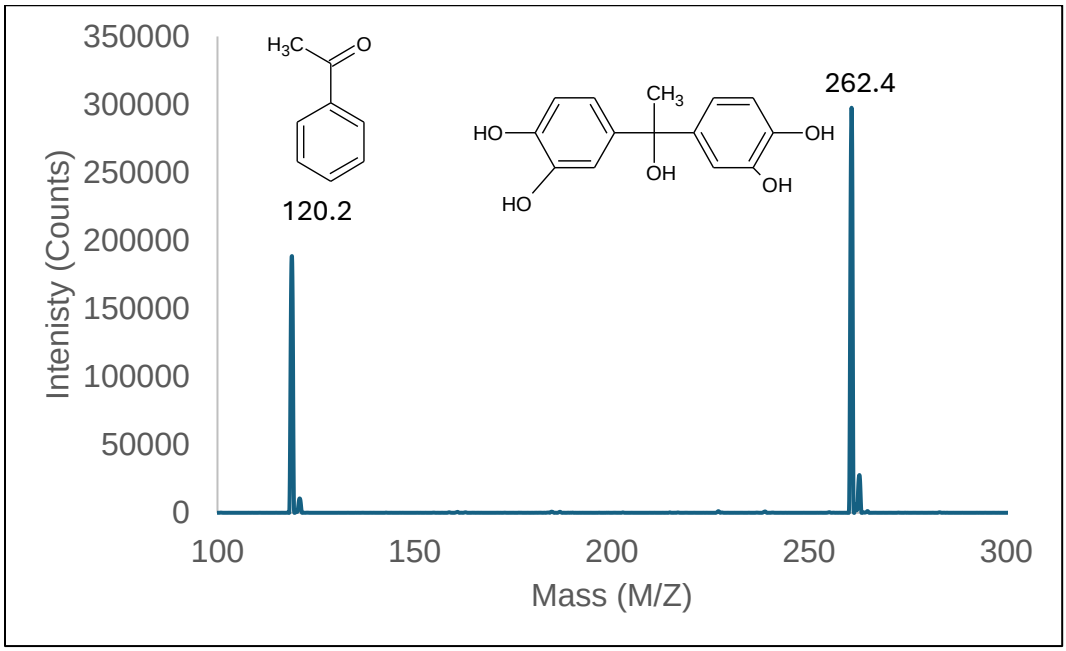

Figure 21: Mass spectra of compound after reaction with the NiS.

The LC-MS was used to determine the breakdown products of the electrocatalytic degradation of BPA using NixSy and CoxSy supported on graphene oxide electrodes.

Figure 16 shows the LC-MS chromatogram of the BPA starting material solution, which consisted of 2 peaks located at retention times (rt) of 101 and 589s. The first peak was determined to consist of one major chemical as can be seen in Figure 17, which had a mass of 262.4 g/mol, which was determined to be a hydroxide modified form of BPA, as can be seen in Figure 17. It is a low intensity peak and is probably an impurity within the compound. Whereas the peak located at 589s was determined to be the BPA, with a mass of 228.21 g/mol a much higher intensity peak Figure 18.

Figure 19 shows the LC-MS chromatogram for the BPA reacted with the electrode in aqueous solution. The intensity of the peak is higher, but at the same retention time only two peaks were visible, this figure is focused on the 101s rt peak. However, with the reacted samples, the peak was determined to consist of two masses, 262.4 g/mol and 120.2 g/mol. The mass of 262.4 g/mol was determined to be 2-bis(3,4-hydroxyphenyl)-1-propanol whereas the mass at 120.2 was determined to be acetophenone as can be seen in Figure 20.

The compound with mass 262.4 g/mol has been identified as 2,2-bis(3,4-hydroxyphenyl)-1-propanol has been observed in the degradation of BPA in the presence of $BiOIO_3$[41]. The 2,2-bis(3,4-hydroxyphenyl)-1-propanol can breakdown through dehydration and ring opening reactions. The process for formation of the compound is shown below, it has been shown to be either a superoxide mechanism or a hydroxyl radical addition.

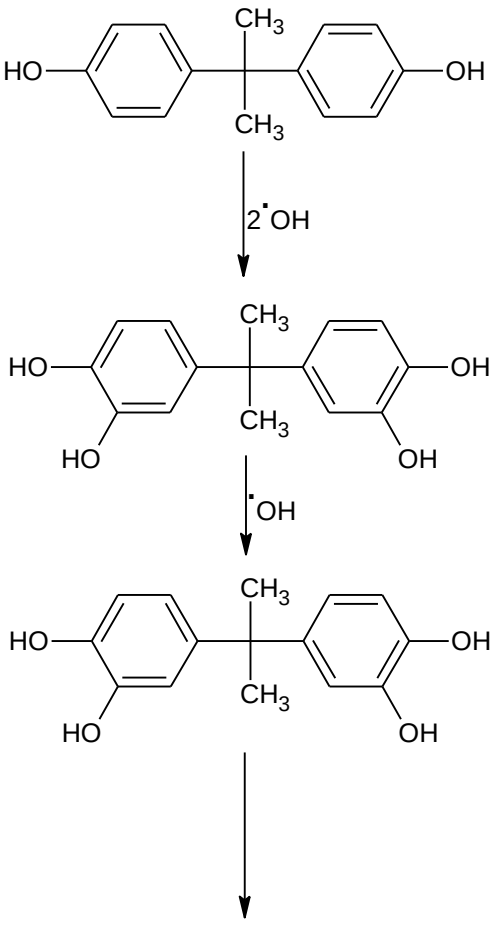

Figure 22: Formation of mass 262.4 during electrolysis.

The compound with mass 120.2 g/mol was identified as acetophenone, which has been observed in the degradation of BPA in the presence of Pseudomonas aeruginosa[40]. The only difference in the reactions with the Co_xS_y (Figure 20) and Ni_xS_y (Figure 21) graphene oxide based electrode was the amount of product produced.

CHAPTER V

CONCLUSIONS

Synthesized NiS/GO and CoS/GO composites were analyzed using X-ray diffraction. The catalysts were studied to monitor the process of degradation of bisphenol A, a persistent organic pollutant, using electrocatalysis. During the investigation, varying parameters of electrolyte concentration, initial pH of BPA solution and initial constant current were applied to maximize catalytic efficiency and determine the optimal conditions for BPA degradation with respect to time.

For both catalysts, an initial pH of 2 demonstrated to be significantly more effective. In a range of pH from 2-6, BPA was most soluble at an initial pH of 2. The BPA degradation process, for both composite materials, had a first order dependence on the BPA concentration in solution, thus proceeding by a first order reaction. The reactions rates for the degradation of BPA by the NiS/GO composite had the highest magnitude at pH 2 (-0.0006 s^{-1}), followed by pH 6 (-3.00E-05 s^{-1}) and then pH 4 (2.00E-05 s^{-1}) and also expressed the highest magnitude at pH 2 (-0.001 s^{-1}), followed by pH 6 (-0.0002 s^{-1}) and then pH 4 (-0.0001 s^{-1}) for the CoS/GO composite. No standard correlation of BPA degradation coupled with increasing concentrations of Na_2SO_4 electrolyte in solution or increasing constant current was observed, therefore added electrolyte and current conditions must be further explored. Under the combination of all altered conditions the CoS/GO composite proved to reduce BPA concentration in the solution more prominently in all cases except for at pH 2, 0.2 A and 4.0 g/L electrolyte resulting in a 2% difference in

concentration when compared to the NiS/GO composite. The experimental results prove the activities of NiS/GO are inferior to those of CoS/GO during the degradation process of BPA with altered conditions in the system.

REFERENCES

1. Sun, P., Liu, X., Zhang, M., Li, Z., Cao, C., Shi, H., Yang, Y., Zhao, Y. Sorption and leaching behaviors between aged MPs and BPA in water: The role of BPA binding modes within plastic matrix. Water Research. 195, (2010) 116956.

2. Heinala,M., Ylinen, K., Tuomi, T., Santonen, T., Porras, S. Annals of Work Exposure and Health, 61(1) (2017), pp. 44-55.

3. Becher, R., Wellendorf, H., Sakhi, A., Samuelsen, J., Thomsen, C., Bølling, A., Kopperud, H. Acta Biomaterialia Odontologica Scandinavica, 4(1) (2018), pp. 56-62.

4. Vilarinho, F., Lestido-Cardama, A., Sendón, R., Quirós, A., Vaz, M., Sanches-Silva, A. Coatings, 10(7) (2020), 624.

5. Kim, S., Chen, J., Cheng, T., Gindulyte, A., He, J., He, S., Li, Q., Shoemaker, B., Thiessen, P.A., Yu, B., Zaslavsky, L. Zhang, J., Bolton, E. E. (2023). PubChem 2023 update. Nucleic Acids Res., 51(D1), D1373-1380.

6. Libretexts, Bisphenol A. *Chemistry LibreTexts* (2023), (available at https://chem.libretexts.org/Ancillary_Materials/Exemplars_and_Case_Studies/Exemplars/Environmental_and_Green_chemistry/Bisphenol_A).

7. Center for Food Safety and Applied Nutrition, Bisphenol A (BPA). *U.S. Food and Drug Administration*, (available at https://www.fda.gov/food/food-packaging-other-substances-come-contact-food-information-consumers/bisphenol-bpa).

8. Melcer, H., Klecka, G. Water Environment Research, 83(7) (2011), pp. 650-666.

9. Goodman, J.E., Peterson, M.K.,Bisphenol A, Encyclopedia of Toxicology 3rd ed., Academic Press, (2014), pp. 514-518.

10. Słomczyńska M. Xenoestrogens: mechanisms of action and some detection studies. Pol J Vet Sci. 2008;11(3):263-9. PMID: 18942551.

11. Česen M., Lenarčič K., Mislej V., Levstek M., Kovačič A., Cimrmančič B., Uranjek N., Kosjek T., Heath D., Dolenc M.S., Heath E. The occurrence and source identification of bisphenol compounds in wastewaters. Sci Total Environ. (2018) pp. 616-617:744-752. PMID: 29096955.

12. Wang, X., Nag, R., Brunton, N., Siddique, A., Harrison, S., Monahan, F., Cummins, E. Human health risk assessment of bisphenol A (BPA) through meat products, Environmental Research, Vol. 213 (2022) 113734.

13. Gorecki, S., Bemrah, N., Roudot, A.C., Marchioni, E., Le Bizec, B., Faivre, F., Kadawathagedara, M., Botton, J., Rivière, G. Human health risks related to the consumption of foodstuffs of animal origin contaminated by bisphenol A, Food and Chemical Toxicology, Vol. 110 (2017), pp. 333-339.

14. Rogers, K., "bisphenol A." *Encyclopedia Britannica*, March 3, 2024.

15. Libretexts, Electrolytic cells. *Chemistry LibreTexts* (2023), (available at https://chem.libretexts.org/Bookshelves/Analytical_Chemistry/Supplemental_Modules_(Analytical_Chemistry)/Electrochemistry/Electrolytic_Cells).

16. Wang, X., Zhao, Y., Tian, E., Li, J., Ren, Y. Graphene Oxide-Based Polymeric Membranes for Water Treatment. Advanced Materials Interfaces, 5(15) (2018), 1701427.

17. N. Abhiram, D. Thangaraju, R. Marnadu, G. Johnsy Arputhavalli, S. Gunasekaran, P. Vetrivelan, N.S.M.P. Latha Devi, Mohd. Shkir, H. Algarni. Structural, vibrational, morphological, optical and electrical properties of NiS and fabrication of SnS/NiS nanocomposite for photodetector applications, Inorganic Chemistry Communications, Vol. 133 (2021), 108882.

18. Jurek, A.; Leitner, E. Analytical Determination of Bisphenol a (BPA) and Bisphenol Analogues in Paper Products by LC-MS/MS. *Food Additives & Contaminants: Part A 35*(11) (2018, pp. 2256–2269.

19. Vengatachalam, M., Ramakrishnan, E., Revathi, P., Palani, S. Efficient photocatalytic degradation of crystal violet by using graphene oxide/nickel sulphide nanocomposites, Bulletin of Materials Science, Research Gate, 43(265) (2020).

20. Flowers, P., Theopold, K., Robinson, W. Chemistry 2e. Rice University. (2019) pp. 599-643.

21. Jain, A., Ong, S.,Hautier, G., Chen, W., Richards, W.D.,Dacek, S., Cholia, S., Gunter, D., Skinner, D., Ceder, G., Persson, K.A. Commentary: The Materials Project: A materials genome approach to accelerating materials innovation, APL Materials, 1(1) (2013), 011002.

22. Petousis, I., Mrdjenovich, D., Ballouz, E., Liu, M., Winston, D., Chen, W., Schladt, T.D., Persson, K.A., High-throughput screening of inorganic compounds for the discovery of novel dielectric and optical materials. *Sci Data* 4 (2017), 160134.

23. Munro, J.M., Latimer, K., Horton, M.K., Dwaraknath, S., Persson, K.A. An improved symmetry-based approach to reciprocal space path selection in ban structure calculations. Computational Materials. Research Gate. 6(1) (2020), pp. 112.

24. Singh, A.K., Zhou, L., Shinde, A., Suram, S.K., Montoya, J.H., Winston, D., Gregoire, J.M., Persson, K.A. Electrochemical Stability of Metastable Materials. Chemistry Materials. ACS Publications. 29(23) (2017) pp. 10159-10167.

25. Patel, A.M., Norskov, J.K., Persson, K.A., Montoya, J.H. Physical Chemistry Chemical Physics 21(45) (2019), pp. 25323-25327.

26. Persson, K.A., Waldwick, B., lazic, P., Ceder, G. Prediction of solid-aqueous equilibria: Scheme to combine first-principles calculations of solids with experimental aqueous states. Phys. Rev. B 85(43) (2012), 235438.

27. Ding, H., Dwaraknath, S.S., Garten, L., Ndione, P., Ginley, D., Persson, K.A. Computational Approach for Epitaxial Polymorph Stabilization through Substrate Selection. ACS Appl. Matr. Interfaces. 8(20) (2016), pp. 13086-13093.

28. Jain, A., Hautier, G., Ong, S.P., Moore, C.J., Fischer, C.C., Persson, K.A., Ceder, G. Formation enthalpies by mixing GGA and GGA + U calculations. Phys. Rev. B 84 (2011), 045115.

29. Aykol, M., Dwaraknath, S.S., Sun, W., Persson, K.A. Thermodynamic limit for synthesis of metastable inorganic materials. Science Advances. 4(4) (2018).

30. Tran, R., Xu, Z., Radhakrishnan, B., Winston, D., Sun, W., Persson, K.A., Ong, S.P. Surface energies of elemental crystals. Sci. Data 3 (2016), 160080.

31. Jong, M., Chen, W., Angsten, T., Jain, A., Notestine, R., Gamst, A., Sluiter, M., Ande, C.K., Zwaag, S., Plata, J.J., Toher, C., Curtarolo, S., Ceder, G., Persson, K.A., Asta, M. Charting the complete elastic properties of inorganic crystalline compounds. Sci. Data 2 (2015), 150009.

32. Zheng, H., Li, X.G., Tran, R., Chen, C., Horton, M., Winston, D., Persson, K.A., Ong, S.P. Grain boundary properties of elemental metals. Acta Materialia 186 (2020), pp. 40-49.

33. Rodriguez-Carvajal, J. Recent advances in magnetic structure determination by neutron powder diffraction. Physica B: Physics of Condensed Matter 192(1-2) (1993), pp. 55-69.

34. Ahmad, Z., Principles of Corrosion Engineering and Corrosion Control. Butterworth-Heinemann. Elsevier (2006), pp. 9-56.

35. Espinosa, S., Bosch, E., Roses, M., Retention of Ionizable Compounds on HPLC. 12. The Properties of Liquid Chromatography Buffers in Acetonitrile-Water Mobile Phases That Influence HPLC Retention. Anal. Chem 74(15) (2002), pp. 3809-3818.

36. Vijayalakshmi, V., Senthilkumar, P., Mophin-Kani, K., Sivamani, S., Sivarajasekar, N., Vasantharaj, S. Bio-degradation of Bisphenol A by Pseudomonas aeruginosa PAb1 isolated from effluent of thermal paper industry: Kinetic modeling and process optimization. Journal of Radiation Research and Applied Sciences, 11(1) (2018), pp. 56-65.

37. Lai, J., Jiang, X., Zhao, M., Cui, S., Yang, J., Li, Y. Thickness-dependent layered BiOIO3 modified with carbon quantum dots for photodegradation of bisphenol A: Mechanism, pathways and DFT calculation. Applied Catalysis B. Environmental 298 (2021), 120622.

VITA

Katherine Ellynn Wright was born in Worcester, Massachusetts. She grew up in Morenci, Arizona and graduated from Eastern Arizona College with an associate in general studies in 2015. She attended Austin College in Sherman, Texas where she played for the softball team, before transferring after two years to The University of Texas Rio Grande Valley and graduated in 2020 with her bachelor's in chemistry. In the spring of 2021 Katherine began the master's degree in chemistry, while conducting research, completing graduate courses, working as a teaching assistant and a full time job outside of school. Ms. Wright graduated with her M.S. degree in Chemistry in May of 2024. Ms. Wright's permanent email address is katherinewright05@gmail.com.